Multi-Mode Dual-Polarized Cavity Backed Patch Antenna Array for 5G Mobile Devices

Paola, Carla di; Zhao, Kun; Pedersen, Gert Frølund; Zhang, Shuai

Published in:
IET Microwaves, Antennas & Propagation

DOI (link to publication from Publisher):
10.1049/mia2.12046

Publication date:
2021

Document Version
Publisher's PDF, also known as Version of record

Received: 29 September 2020 | Revised: 26 November 2020 | Accepted: 14 December 2020

IET Microwaves, Antennas & Propagation

DOI: 10.1049/mia2.12046

ORIGINAL RESEARCH PAPER

Multi-mode dual-polarised cavity backed patch antenna array for 5G mobile devices

Carla Di Paola[1] | Kun Zhao[1,2] | Gert F. Pedersen[1] | Shuai Zhang[1]

[1]Antennas, Propagation and mm-Wave Systems (APMS) Section, the Department of Electronic Systems, Aalborg University, Aalborg, Denmark

[2]Research Center Lund, Sony Corporation, Lund, Sweden

Correspondence

Shuai Zhang, Antennas, Propagation and mm-Wave Systems (APMS) Section, the Department of Electronic Systems, Aalborg University, Aalborg 9100, Denmark.
Email: sz@es.aau.dk

Funding information

Innovation Fund Denmark; WiSpry; AAC; Sony Mobile; AAU young talent programme

Abstract

This paper proposes a dual-polarised cavity backed patch antenna for next generation phased arrays for mobile handsets. The antenna exhibits multi-band performance, allowing to cover the 5G bands n257 (26.5–29.5 GHz), n258 (24.25–27.5 GHz), n261 (27.5–28.35 GHz) and a portion of band n260 (37–40 GHz). Two orthogonal modes are excited in the substrate integrated waveguide (SIW) cavity and show similar impedance matching and symmetric radiation patterns. A parasitic element is introduced on top of the cavity and shifted off-centre to improve the port-to-port isolation and guide the main beam. A parametric study of the antenna dimensions is conducted to verify the multi-resonance operating mechanism. The design is validated by the measurements of the fabricated four-element array. The array scanning angle is from −35° to 38° for V-pol and from −29° to 31° for H-pol at 28 GHz, where the realised gain raises from 8 to 12 dBi.

1 | INTRODUCTION

The millimetre-wave bands provide wide bandwidths that can support higher speed data transfer and massive device connectivity required by the upcoming fifth generation mobile communication system (5G) [1–4]. However, by increasing the operating frequency, the propagation loss becomes more significant, according to the Friis transmission equation [5]. Therefore, high gain antenna systems are proposed to be embedded in mobile terminals to compensate the larger path loss, transmission loss, shadowing loss and user blockages [6,7]. Since high gain leads to narrow radiation beamwidth, beam-steerable phased arrays result good candidates, thanks to their ability to realise beam forming and achieve a large coverage range [8–10]. Moreover, due to the limited space reserved in mobile handsets for the antenna, beam-steerable phased arrays are required to be compact in size.

Planar and low-profile antennas have contributed significantly towards miniaturisation, for example microstrip patch antennas. However, microstrip patch antennas suffer from narrowband impedance matching, resulting from the small separation between the patch and the ground plane, and low gain, due to the surface waves that distort the radiation pattern [11,12]. Therefore, to make them suitable radiators for the emerging technologies, the patch antenna is buried into a metallic cavity [13]. This technology has the potential to widen the limited bandwidth of the conventional patch antenna, by increasing the volume under the patch. Additionally, the cavity enhances the antenna gain and radiation efficiency, as it is very effective in suppressing surface waves and backlobes, typical of finite ground plane patch antenna, improves cross-polar levels in radiation patterns and reduces mutual coupling between antenna elements [14–16]. The extensive study in Reference [17] analyses the influence of every design parameter on the cavity backed antenna performance. A low profile cavity backed antenna realised by multilayer printed circuit board (PCB) structure is first presented in Reference [18], in which the cavity is constructed by two rows of vias connecting upper and lower ground plane. In Reference [19], a cavity backed antenna is first developed using the substrate integrated waveguide (SIW) technology, where the cavity is emulated using array of plated through via holes and the entire structure is fabricated on a single layer substrate. Low-profile SIW cavity-backed antennas are proposed in References [20–24], to realise bandwidth enhancement in X-band, Ku-band, mm-wave and 60 GHz band, respectively. Moreover, they are implemented in References [25,26] for dual linear polarisation applications. In fact, over the past years, dual-polarised antenna arrays have drawn antenna engineers attention, as they allow to cope with the unpredictable polarisation of incoming signals and guarantee a better connection with base stations. Overall, the 5G millimetre-wave system demands dual-polarised antenna arrays, able to operate over a wide bandwidth.

In this paper, a dual-polarised cavity backed stacked patch antenna, with multi-band and high gain performance, and its array of four elements are proposed to cover the bands of the 5G spectrum [27]. The antenna is fed by two orthogonal microstrip lines, exciting two orthogonal modes in the SIW cavity. The initial design suffers from low port-to-port isolation and titled radiation patterns at certain frequency bands, due to the impact of the cavity. Therefore, a novel design on the parasitic patch element is proposed in this work. Different from conventional stacked patch antenna [28], the parasitic patch element, placed on top of the cavity, is shifted off-centre, to increase the cross-polarisation isolation and direct the main beam towards the normal direction. In the final design, the orthogonal modes exhibit the same impedance matching and symmetric radiation patterns.

The paper is organised as follows. The design of the structure is presented in Section II. In Section III, the performance analysis is conducted, followed by the parametric study in Section IV, performed with the electromagnetic simulator CST Microwave Studio 2019. The simulated and measured results of the fabricated array are compared and discussed in Section V. Finally, conclusion is provided in Section VI.

To avoid potential confusion, the main beam is radiated towards the $+z$ direction; the vertical polarisation (V-pol) and the horizontal polarisation (H-pol) correspond to the θ and ϕ polarisation, respectively.

2 | ARRAY ELEMENT STRUCTURE

The array element structure in Figure 1 consists of a three-layers of stack-up PCB. Two layers of Rogers RO4003C (thickness = 0.406 mm, $\epsilon_r = 3.55$, $\tan_\delta = 0.002$) and a layer of Rogers RO4350B (thickness = 0.101 mm, $\epsilon_r = 3.66$, $\tan_\delta = 0.0037$) are connected by two prepreg layers of Rogers RO4450F (thickness = 0.202 mm, $\epsilon_r = 3.52$, $\tan_\delta = 0.004$), as shown in Figure 1a. Four rows of metallised vias, connecting upper and lower layers, form the sidewalls of the square SIW cavity. Buried in the centre of the cavity, the radiating square patch (M2) is printed at the bottom of the second layer of Sub.1. The ground plane (M3) follows below, placed on top of Sub.2. Two orthogonal microstrip lines (M4), located on the bottom of the cavity (bottom of Sub.2), are connected to the patch through plated vias, to excite two orthogonal modes. Waveguide ports 1 and 2 are selected for the V- and H-mode, respectively. In particular, the feeding points are off-centre, that is the V-mode is excited near the right edge of the patch, and the H-mode is fed near the down edge of the patch, resulting in a tilted radiation pattern. To face the problem, a parasitic element, a square plate (M1) is added on top of the cavity (top of first layer of Sub.1), and shifted 0.3 mm diagonally from the centre to the upper left corner. The structure of each layer is presented in detail in Figure 1c, and the depth of feeding and cavity vias is shown in the cross section view in Figure 1b. Dimensions are listed in Table 1.

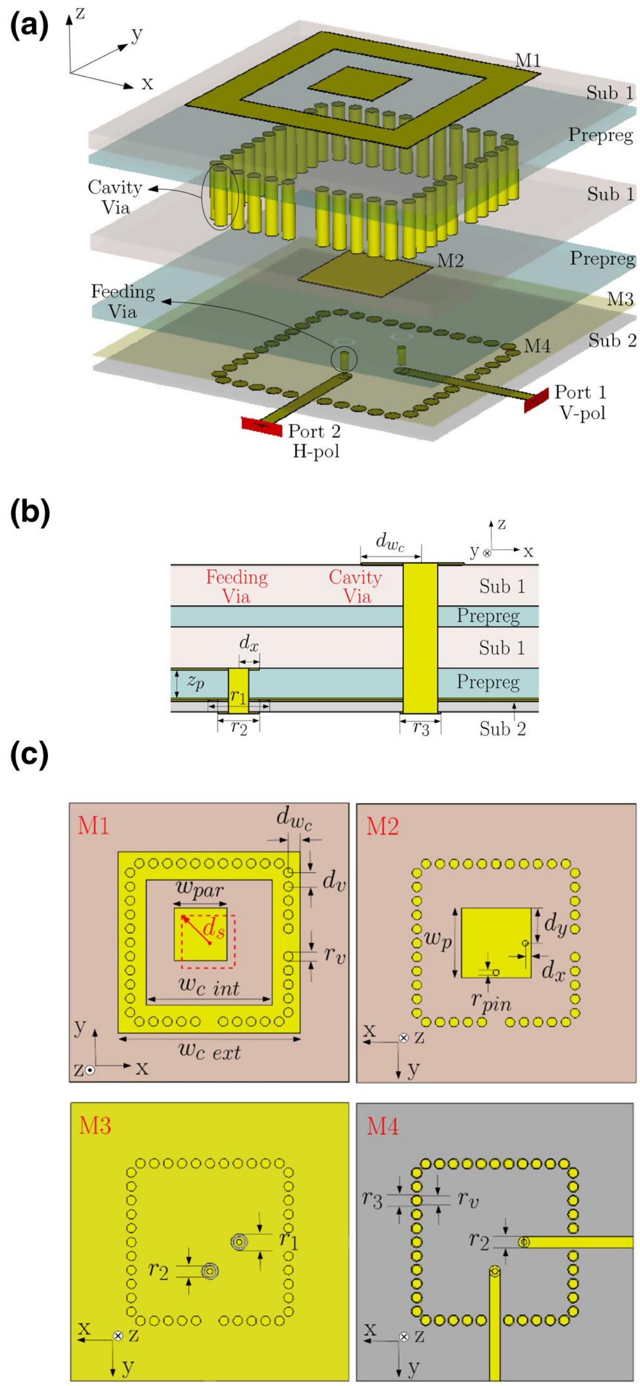

FIGURE 1 Geometric structure of the proposed cavity backed patch antenna for 5G mobile-phones. (a) Exploded and (b) cross sectional view, and (c) layers in detail

TABLE 1 Dimensions of the antenna parameters (Units: mm)

Par.	Value	Par.	Value	Par.	Value
d_s	0.3	r_1	0.6	w_p	2.6
d_x	0.2	r_2	0.4	w_{par}	1.9
d_y	1.3	r_3	0.4	$w_{c\ ext}$	6.5
d_v	0.5	r_{pin}	0.2	$w_{c\ int}$	4.5
d_{w_c}	0.425	r_v	0.34	z_p	0.303

3 | ANTENNA ELEMENT PERFORMANCE

In this section, the antenna operation mechanism will be explained first, and then, the effect of shifting the parasitic element off-centre will be illustrated.

3.1 | Cavity impact

To prove the bandwidth enhancement of the proposed design, the impedance bandwidth of the equivalent patch antenna (see point 1 in Figure 2a) and cavity backed antenna

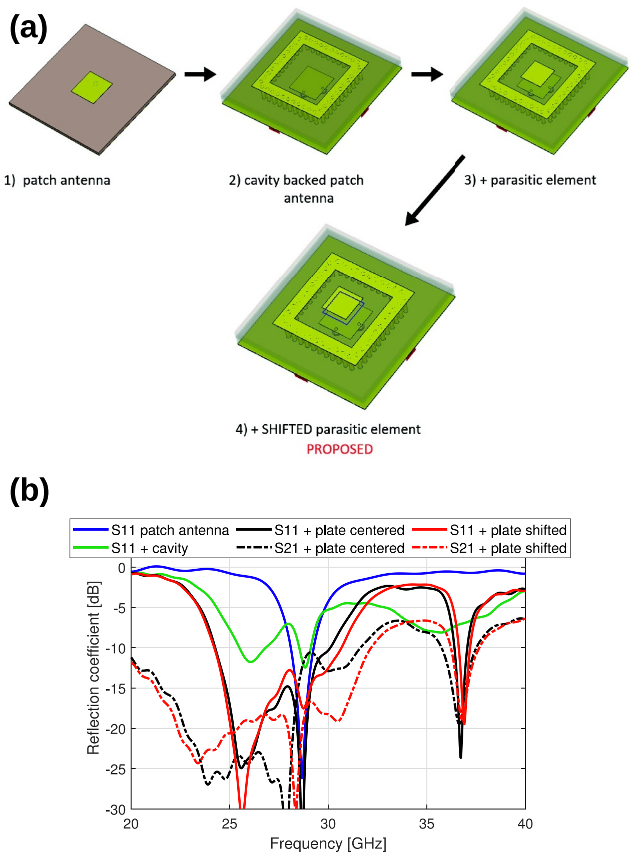

FIGURE 2 (a) Design evolution of the proposed cavity backed patch antenna and (b) corresponding simulated S-parameters. Due to the symmetric structure, S_{22} is similar to S_{11}

(see point 2 in Figure 2a) are juxtaposed in Figure 2b. The first step is to bury the patch into a cavity (point 2 in Figure 2a), exciting a cavity mode close to the resonance of the patch. The surface current distribution evaluated at the resonance frequency of 25.5 GHz in Figure 3a highlights that the patch is responsible of the first mode, while the second mode depends on the cavity, as proved by the current distribution at 28.7 GHz in Figure 3b. The advantages given by the cavity in terms of radiation performance can be observed comparing Figure 5a,b. The radiation pattern of the patch antenna results distorted by the surface waves induced on the substrate and exhibits low realised gain of 6 dBi. The presence of the cavity is very effective in suppressing the surface waves, and thus focus the radiated beam towards the $+z$ direction, shaping a narrow radiation pattern with peak gain of 8.4 dBi.

3.2 | Impact of the parasitic element

The second goal is to improve the impedance matching. Therefore, a parasitic element is placed on top of the cavity in the centre (point 3 in Figure 2a), and another mode is excited at 37 GHz (solid black curve), as confirmed by the surface currents distribution in Figure 3c. The realised gain also benefits from the parasitic element that allows to achieve 9 dBi (Figure 5c). However, this configuration suffers from low isolation between the two ports at 28 GHz (dashed black curve). Moreover, as the feeding is off-centre of the cavity. The radiation pattern at 28 GHz leans to one side, as illustrated in Figure 5c.

3.3 | Shifted parasitic element

Tilted radiation pattern and low port-to-port isolation are solved by shifting the parasitic element off-centre (point 4 in Figure 2a). To demonstrate the benefit for the isolation from the shift, the surface current distribution in the configurations with central and shifted parasitic element is compared in Figure 4. With the plate shifted, the current transferred to port 2 (H-mode), when port 1 (V-mode) is fed, is much lower than in the central placement. Figure 5d proves the effectiveness of the shift on the radiation pattern, resulting in the main beam pointing the normal direction. Therefore, the final design achieves a -10 dB impedance matching from 24.2 to 30.7 GHz, covering the 5G bands n257, n258, n261 and from 37 to 37.8 GHz, which is a portion of band n260, with port-to-port isolation better than -15 dB.

Figure 6 shows the radiation characteristic of the two polarisation modes at 28 GHz. In the vertical plane (yoz), the co-polarised gain of the V-mode is 8.7 dBi, of the H-mode 8.9 dBi and the cross-pol level is more than 10 dB lower than the co-pol for both modes (Figure 6a). Observing the results in the horizontal plane in Figure 6b, co-pol and cross-pol of V-mode and H-mode are symmetric to the opposite polarisation in the vertical plane.

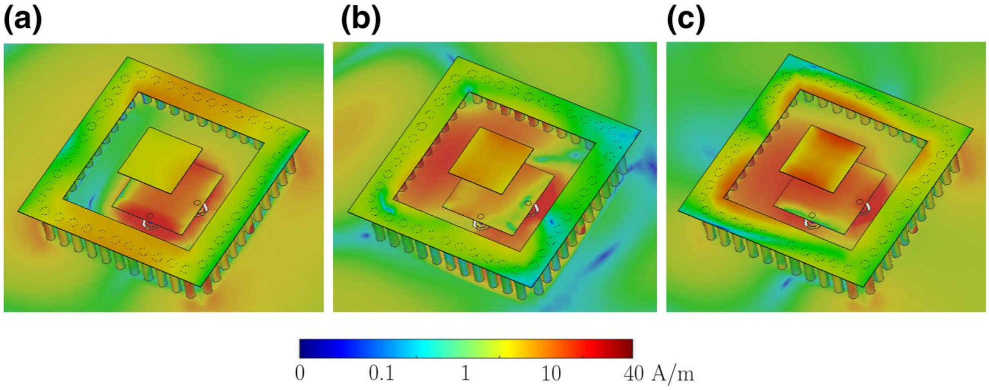

FIGURE 3 Current distribution evaluated at the resonant frequency points of the red curve in Figure 2b: (a) 25.5 GHz, (b) 28.7 GHz and (c) 37 GHz

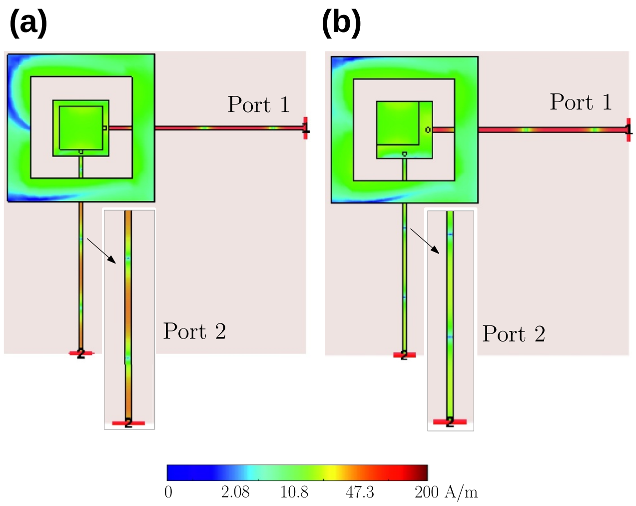

FIGURE 4 Current distribution on the microstrip feeding line two (zoomed), evaluated at 28 GHz in the configurations with (a) central and (b) shifted parasitic element, when port one is fed

4 | PARAMETRIC STUDY

To verify the multi-resonance operating mechanism of the antenna and how the dimensions influence the bandwidth performance, a parametric study is performed using CST. When one parameter is studied, the others are kept to the optimised values. As seen in Figure 2b, three modes are excited.

The dimensions of the patch determine the first resonance and the impedance matching. In fact, as demonstrated in Figure 7a, the patch dimensions are inversely proportional to the resonant frequency and highly affect the impedance matching in low band, that is bigger patch deteriorates the impedance matching, while the high band results unaltered. It can be seen that the optimised value allows to achieve the desired coverage, from the beginning of band n258.

As is widely known, the variation of operational bandwidth is influenced by the distance between the patch and the ground plane. A reduced distance leads to a narrower bandwidth, and the effect is visible in Figure 7b. The value selected represents a trade-off between the bandwidth in low band and the impedance matching in high band.

Though the operating frequency of the proposed antenna is primarily determined by patch size, cavity dimension is an important tuning element to achieve the optimum impedance matching. From Figure 7c, it can be observed that II and III modes are in inversely proportion to cavity dimensions, that is, as cavity size is increased, both modes shift down, leading to a better impedance matching but reduced bandwidth. So, the dimensions of the cavity are adjusted to the appropriate value that guarantees the desired coverage bandwidth with a good impedance matching.

The parasitic element size is another critical parameter, whose effects on resonant frequency and bandwidth are shown in Figure 7d. It results that I and III modes are sensitive to its dimensions, and, in particular, a smaller plate determines a higher resonance for both modes. The chosen value guarantees good impedance matching in low and high bands and allows to cover the whole band n257.

A deeper investigation is conducted on the parasitic element shift, evaluating both return loss and port-to-port isolation. The selected value is compared with different values of shift from the central. Considering the central position as a reference, the progressive shift of the plate determines a better matching in low band and consequently wider bandwidth, as shown in Figure 8a. As previously demonstrated, the patch influences the third mode and, in particular, a further shift generates a higher resonance. Concerning the negative shift, that is moving the plate closer to the feeding points, poor impedance matching is achieved in low band, whereas the resonance in high band overlaps the one given by the same shift in the opposite direction. Comparing the curves in Figure 8b, it results that the selected shift and the smaller one allow to increase the isolation in the interval 28.5−30 GHz, while keeping −15 dB in the bands of interest. The selected shift guarantees both better isolation and good impedance matching till the upper limit of band n257.

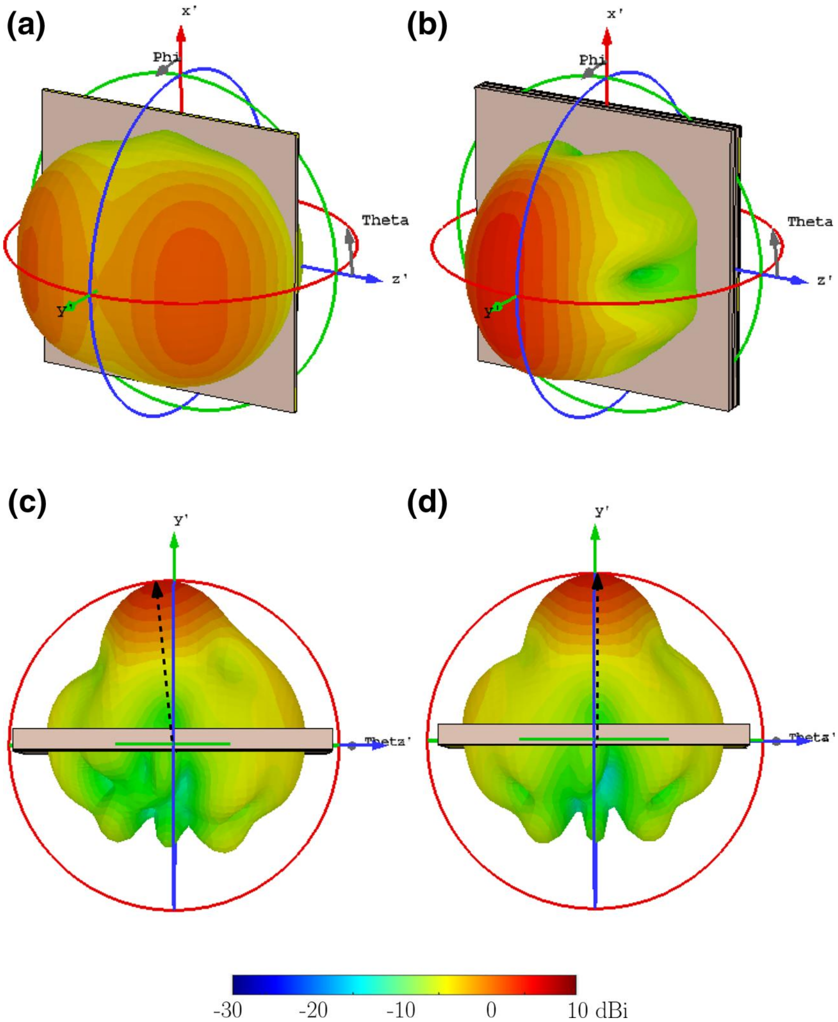

FIGURE 5 Comparison of the simulated radiation pattern at 28 GHz of (a) the patch antenna with (b) the cavity backed patch antenna. In (c), the parasitic element is added in central position and in (d) is shifted off-centre

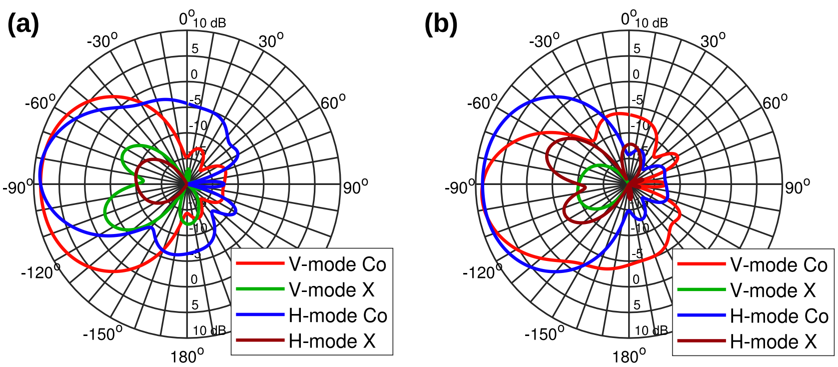

FIGURE 6 Simulated realised gain at 28 GHz (a) in the vertical plane (yoz) and (b) in the horizontal plane (xoz)

5 | ANTENNA ARRAY AND MEASUREMENTS RESULTS

The array of four elements is simulated using the stacked substrate with the length of 35 mm and the width of 70 mm. The element distance is 5.65 mm, which is close to half wavelength of 28 GHz. The array configuration requires the microstrip line feeding the V-pol to be rearranged, in order to place the MMPX connectors, breaking thus the symmetry of each element, with consequent misalignment between the current distribution on the feed and the polarisation for the V-mode case. In order to evaluate if the rearrangement of the V-mode feeding line impacts on the radiation characteristics, array element 4 is simulated with the V-pol feeding line both orthogonal and parallel to the H-pol feeding line. However, the results demonstrate that the placement of the feeding line does not alter the radiation pattern generated by the V-mode. On the other hand, as opposed to the single element

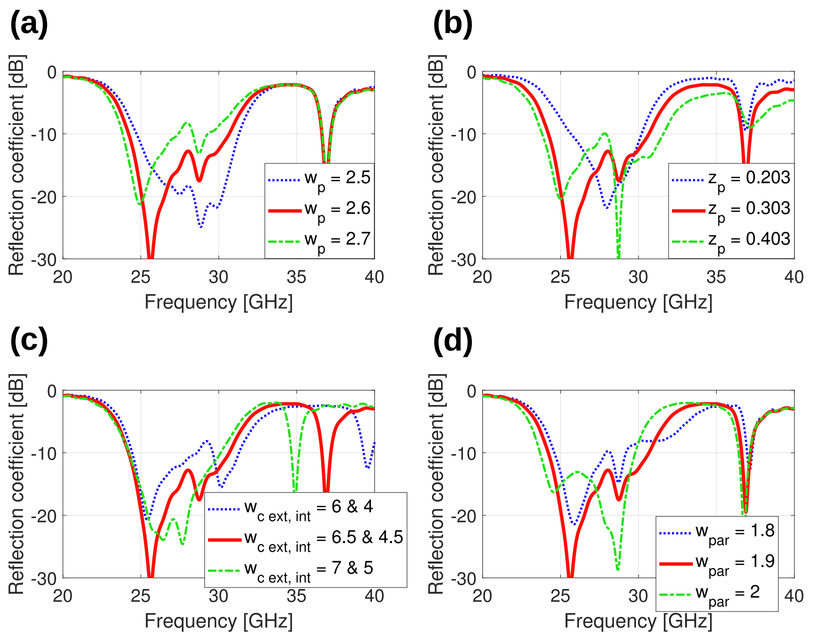

FIGURE 7 S_{11} of the proposed antenna versus (a) patch size, (b) patch position, (c) cavity dimensions and (d) parasitic element dimensions

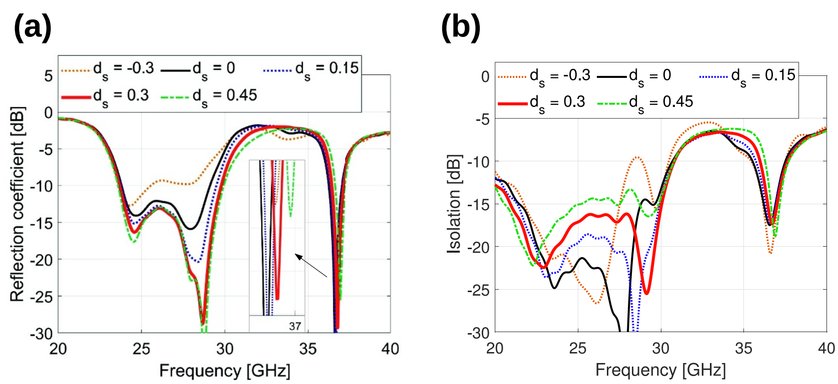

FIGURE 8 (a) S_{11} and (b) S_{21} of the proposed antenna versus parasitic element shift

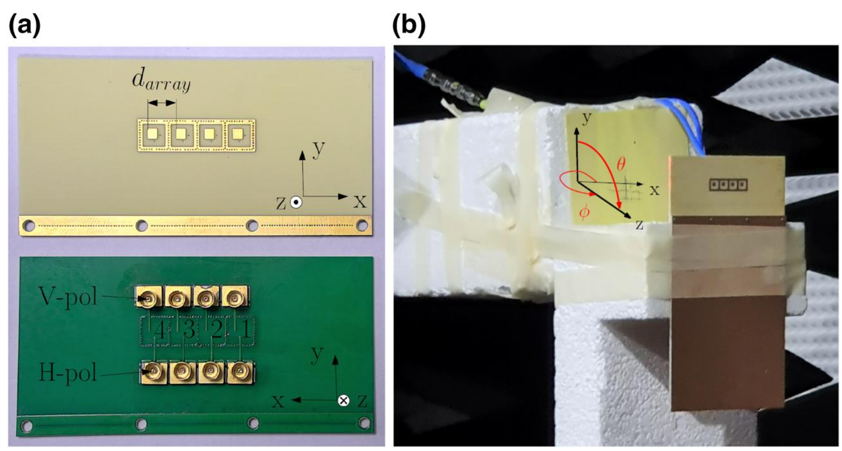

FIGURE 9 Fabricated antenna array (a) top and bottom view and (b) measurements setup in the anechoic chamber

characteristics, V_1 and H_1 in Figure 10a, representing the reflection coefficients of the V-pol and H-pol ports of array element 1, respectively, are slightly different from each other, and another resonance is generated at 31 GHz. Simulations results prove that other offsets of the parasitic patch (d_s) can provide better cross-polarisation isolation, but the offset value $d_s = 0.3$ mm is still selected for the fabricated prototype to ensure the peak radiation pointing towards the normal

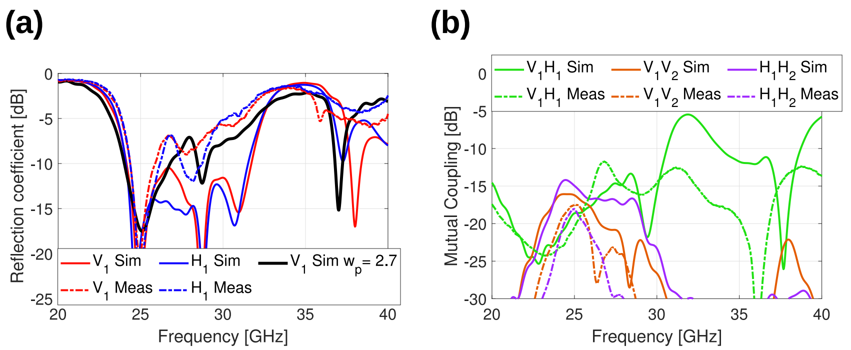

FIGURE 10 Comparison of the simulated and measured (a) return loss and (b) mutual coupling of array element 1. The other array elements have similar performance, so the results are omitted for simplicity. In (a), the return loss of array element 1 with bigger patch is reported to justify the discrepancy between simulations and measurements

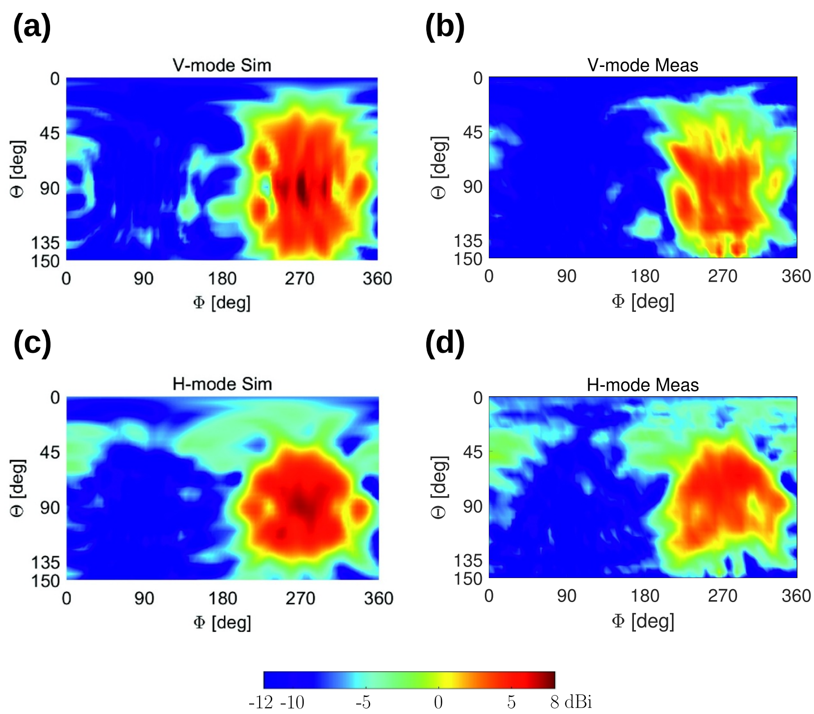

FIGURE 11 Comparison of the simulated and measured 3D radiation pattern of array element 1 at 28 GHz. (a) Simulated and (b) measured V-mode. (c) Simulated and (d) measured H-mode. The other array elements have similar performance, so the results are omitted for simplicity

direction, while providing decent isolation performance over the entire bandwidth.

Figure 9a shows the fabricated prototype. S-parameters are measured using the Keysight N5227A PNA Microwave Network Analyser and compared with full wave simulated results as shown in Figure 10. Simulated and measured curves of the return loss (Figure 10a) follow the same trend, even though the second mode generated by the cavity and the one in band n260 related to the parasitic element are not matched below − 10 dB. Based on the parametric study conducted in Section 4, simulations with different parameters dimensions are performed, in order to investigate the discrepancy. It turns out that the realised component has a bigger patch, responsible of the degraded impedance matching, as confirmed by the return loss of the V-mode of antenna 1, simulated with $w_p = 2.7$ mm, juxtaposed in Figure 10a. The measured isolation between the V-pol and the H-pol ports, V_1H_1 in Figure 10b, is in agreement with the simulated. V_1V_2 and H_1H_2, the coupling between the V-pol ports and H-pol ports, respectively, of array element 1 and 2, are both below −15 dB.

Figure 9b shows the measurements setup in the anechoic chamber located at Aalborg University. The antenna under test, mounted on the short edge of the phone ground plane to emulate a realistic scenario, is installed on a platform that rotates 360° along ϕ, while a mechanical arm, where a measuring probe is fixed, turns from 0° to 150° along θ. Each antenna element is measured at a time, and the rest of the elements are loaded with 50 Ω. The 3D far-field radiation patterns of V- and H-modes measured at 28 GHz are depicted in Figure 11. The measured radiation patterns match the simulated, and the beam scanning along θ and ϕ is confirmed, despite a decrease in gain of approximately 3 dB is observed for both modes, that can be ascribed to the impedance mismatch at the selected frequency point, due to the antenna mockup fabrication issues, as explained above, as well as to extra ohmic loss in the prototype of about 1.5 dB compared to the simulations.

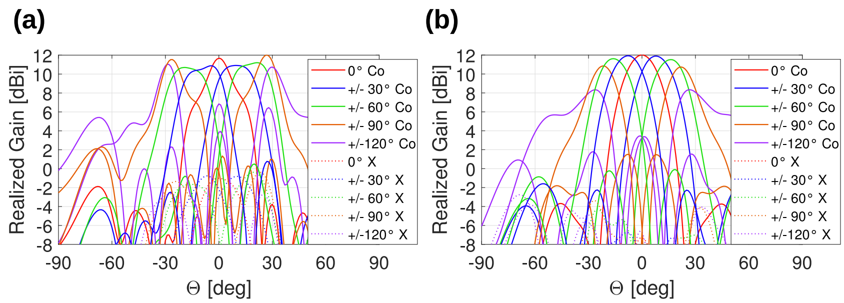

FIGURE 12 Simulated scanning patterns in the horizontal plane (xoz) of (a) V-mode and (b) H-mode at 28 GHz. For ϕ varying from 180° to 360°, the corresponding value at $\theta = 90°$ is plotted

The resulting simulated beam-steering envelope in the H-plane at 28 GHz is shown in Figure 12. The envelope is obtained by the realised gain of nine beams, generated by the progressive phase shifts of 0°, ±30°, ±60°, ±90° and ±120°. If we define the scanning angle as a relative range to the peak value, 12 dBi, the V-mode can cover from −35° to 38° and the H-mode from −29° to 31° with 4 dB degradation. The envelope of the H-mode in Figure 12b is homogeneous, and the gain decreases gradually from the peak value at 0°. On the other hand, the envelope of the V-mode in Figure 12a shows three peak values at 0° and ±25°. The presence of three peaks in the array pattern is justified by the three peaks in the element pattern, as shown in Figure 11a, since the array pattern is the product of element pattern and array factor. The distorted scanning pattern generated by the V-mode is due to the placement of the array elements along the V-polarisation, which determines a stronger impact from the neighbouring array elements on each element radiation pattern and further results into the distortion on the beam scanning pattern, as can be observed in Figure 12a.

6 | CONCLUSION

A cavity backed patch antenna, with dual-polarization and multi-band performance, is proposed to cover the 5G bands from 24.25 to 29.5 GHz and from 37 to 37.8 GHz. Novel component of the design is the parasitic element, shifted off-centre on top of the cavity, that improves the isolation between the two polarisations and addresses the main beam to the normal direction. A four-element array is implemented with the proposed antenna as array elements. The measured far-field radiation patterns are in accordance with the simulations, though a decrease in gain of 3 dB on average is detected. The array scanning angle is from −35° to 38° for V-pol and from −29° to 31° for H-pol, where the realised gain reaches 12 dBi at 28 GHz. Future work aims to exploit different technologies to minimise the antenna profile, while keeping wideband and high gain performance.

ACKNOWLEDGEMENTS

This work was conducted under the framework of the Reconfigurable Arrays for Next Generation Efficiency (RANGE) project, supported by the Innovation Fund Denmark together with industry partners: WiSpry, AAC and Sony Mobile, and is co-financed by the AAU young talent programme. The authors would like to thank lab engineers Ben Kroeyer, for valuable guidance in the realization of the prototype, and Kristian Bank and Kim Olesen, for precious assistance in the measurements setup.

ORCID

Carla Di Paola https://orcid.org/0000-0003-0509-2832

REFERENCES

1. Rappaport, T.S., et al.: Broadband millimeter-wave propagation measurements and models using adaptive-beam antennas for outdoor urban cellular communications. IEEE Trans. Antennas Propag. 61(4), 1850–1859 (2012)
2. Bai, T., Heath, R.W.: Coverage and rate analysis for millimeter-wave cellular networks. IEEE Trans. Wireless Commun. 14(2), 1100–1114 (2015)
3. Wang, C.X., et al.: Cellular architecture and key technologies for 5g wireless communication networks. IEEE Commun. Mag. 52(2), 122–130 (2014)
4. Pi, Z., Khan, F.: An introduction to millimeter-wave mobile broadband systems. IEEE Commun. Mag. 49(6) (2011)
5. Balanis, C.A.: Antenna Theory: Analysis and Design. John Wiley & Sons (2016)
6. Rajagopal, S., et al.: Antenna array design for multi-gbps mmwave mobile broadband communication. In: Global Telecommunications Conference (GLOBECOM), pp. 1–6. IEEE (2011)
7. Zhao, K., et al.: User body effect on phased array in user equipment for the 5g mmwave communication system. IEEE Antennas Wirel. Propag. Lett. 16, 864–867 (2016)
8. Hong, W., et al.: Study and prototyping of practically large-scale mmwave antenna systems for 5g cellular devices. IEEE Commun. Mag. 52(9), 63–69 (2014)
9. Hong, W., et al.: Multibeam antenna technologies for 5g wireless communications. IEEE Trans. Antennas Propag. 65(12), 6231–6249 (2017)
10. Roh, W., et al.: Millimetre-wave beamforming as an enabling technology for 5g cellular communications: Theoretical feasibility and prototype results. IEEE Commun Mag. 52(2), 106–113 (2014)
11. James, J.R., et al.: Handbook of Microstrip Antennas. 1, IET (1989)
12. Garg, R., et al.: Microstrip antenna design handbook. Artech House (2001)
13. Karmakar, N.C.: Investigations into a cavity-backed circular-patch antenna. IEEE Trans. Antennas Propag. 50(12), 1706–1715 (2002)
14. Navarro, I., Kai, C.: A ka-band cavity-enclosed aperture-coupled circular patch antenna and array for millimeter-wave circuit integration. In: IEEE Antennas and Propagation Society International Symposium 1992 Digest, pp. 313–316. IEEE (1992)
15. Aberle, J.T.: On the use of metallised cavities backing microstrip antennas. In: Antennas and Propagation Society Symposium 1991 Digest, pp. 60–63. IEEE (1991)
16. Brynjarsson, B., Syversen, T.: Cavity-backed, aperture coupled microstrip patch antenna. In: 1993 Eighth International Conference on Antennas and Propagation, pp. 715–718. IET (1993)
17. Awida, M., Fathy, A.E.: Design guidelines of substrate-integrated cavity-backed patch antennas. IET Microw. Antennas Propag. 6(2), 151–157 (2012)

18. Locker, C., Vaupel, T., Eibert, T.F.: Radiation efficient unidirectional low-profile slot antenna elements for x-band application. IEEE Trans. Antennas Propag. 53(8), 2765–2768 (2005)
19. Luo, G.Q., et al.: Planar slot antenna backed by substrate integrated waveguide cavity. IEEE Antennas Wireless Propag. Lett. 7, 236–239 (2008)
20. Luo, G.Q., et al.: Bandwidth-enhanced low-profile cavity-backed slot antenna by using hybrid siw cavity modes. IEEE Trans. Antennas Propag. 60(4), 1698–1704 (2012)
21. Awida, M.H., Fathy, A.E.: Substrate-integrated waveguide ku-band cavity-backed 2 × 2 microstrip patch array antenna. IEEE Antennas Wirel. Propag Lett. 8, 1054–1056 (2009)
22. Yang, T.Y., Hong, W., Zhang, Y.: Wideband millimeter-wave substrate integrated waveguide cavity-backed rectangular patch antenna. IEEE Antennas Wirel. Propag. Lett. 13, 205–208 (2014)
23. Li, Y., Luk, K.M.: 60-GHz substrate integrated waveguide fed cavity-backed aperture-coupled microstrip patch antenna arrays. IEEE Trans. Antennas Propag. 63(3), 1075–1085 (2015)
24. Gong, K., et al.: Substrate integrated waveguide cavity-backed wide slot antenna for 60-GHz bands. IEEE Trans. Antennas Propag. 60(12), 6023–6026 (2012)
25. Luo, G.Q., et al.: Development of low profile cavity backed crossed slot antennas for planar integration. IEEE Trans. Antennas Propag. 57(10), 2972–2979 (2009)
26. Paryani, R.C., Wahid, P.F., Behdad, N.: A wideband, dual-polarized, substrate-integrated cavity-backed slot antenna. IEEE Antennas Wirel. Propag. Lett. 9, 645–648 (2010)
27. 3GPP TR 38. 817-01. General aspects for user equipment (UE) radio frequency (RF) for NR (Release 15). 3GPP (2019)
28. Hwang, I.J., et al.: Cavity-backed stacked patch array antenna with dual polarization for mmwave 5g base stations. In: 13th European Conference on Antennas and Propagation (EuCAP), pp. 1–5. IEEE (2019)

How to cite this article: Di Paola C, Zhao K, Pedersen GF, Zhang S. Multi-mode dual-polarised cavity backed patch antenna array for 5G mobile devices. *IET Microw. Antennas Propag.* 2021;15:280–288. https://doi.org/10.1049/mia2.12046